IOP Publishing Journal of Physics: Condensed Matter
J. Phys.: Condens. Matter **32** (2020) 145601 (7pp) https://doi.org/10.1088/1361-648X/ab6021

Majorana corner modes in an s-wave second order topological superfluid

Ya-Jie Wu[1,4], Tan-Biao Gao[1], Ning Li[1], Jiang Zhou[2] and Su-Peng Kou[3]

[1] School of Science, Xi'an Technological University, Xi'an 710032, People's Republic of China
[2] Department of Physics, Guizhou University, Guiyang 550025, People's Republic of China
[3] Department of Physics, Beijing Normal University, Beijing 100875, People's Republic of China

E-mail: wuyajie@xatu.edu.cn

Received 15 July 2019, revised 3 December 2019
Accepted for publication 9 December 2019
Published 6 January 2020

Abstract

In sharp contrast to conventional topological superfluids, higher order (order $r > 1$) topological superfluids in n dimensions do not host $n-1$ dimensional Majorana boundary states, instead host $n-r$ dimensional Majorana excitations. In this paper, we propose Majorana corner modes can emerge in a second order superfluid with s-wave pairing, instead of unconventional pairings such as d-wave and $s_{\pm}$-wave pairings in most of previous proposals. There are three key ingredients in this scheme consisting of a topological insulator, an in-plane Zeeman field, and an s-wave pairing. Based on the low energy theory for edge states, where the effective Dirac mass sign changes at the corner, we unveil the emergence of Majorana corner modes. Our proposal provides a promising platform for implementing 2D second order topological superfluids and Majorana corner modes.

Keywords: Majorana corner modes, second order topological superfluids, s-wave pairing

(Some figures may appear in colour only in the online journal)

1. Introduction and motivation

Topological superfluids (TSFs) and topological superconductors (TSCs) are a class of topologically non-trivial quantum states [1, 2]. Based on local symmetries, i.e. particle-hole symmetry ($\mathcal{P}$), time-reversal symmetry ($\mathcal{T}$) and chiral symmetry ($\mathcal{C}$), two dimensional TSFs and TSCs are classified into three categories consisting of D-type, C-type and DIII-type ones [3–5]. Owing to the bulk-boundary correspondence, the topological invariant characterizing bulk topology can predict the number of edge states and chirality. For instance, the integer topological number $\mathbb{Z}$ in class D counts the number of chiral Majorana edge modes. The local symmetries $(\mathcal{P},\mathcal{T},\mathcal{C})$ successfully capture topological nature of general physical systems. Whereas spatial symmetries, such as translation and point group symmetries, can also lead to nontrivial bulk topology and boundary states for selected surfaces or edges [6–9]. Moreover, the mirror-reflection-symmetry protected surface gapless states have been observed in experiments [10, 11]. Motivated by these progresses, various TSC and TSFs with spatial symmetries (translation, inversion, reflection and other point symmetries) have been elucidated [12–16]. Furthermore, the symmetry-protected Majorana zero modes are predicted in the unconventional spinful TSFs and TSCs [15, 16].

Recently, a new class of TSCs, called higher order TSCs, have been proposed [17–25]. r ($r \geqslant 2$) order TSCs in d dimensions host $d-r$ dimensional Majorana boundary states rather than $d-1$ dimensional gapless Majorana excitations in conventional TSCs. For instance, for the the second order TSC in two dimensions, Majorana corner modes (MCMs) localize at the intersection between adjacent boundaries. Recently, a variety of schemes have been proposed to implement second order TSCs, such as $(p_x+\mathrm{i}p_y)\times(p_x-\mathrm{i}p_y)$-wave superconductors with a magnetic field [20], 2D topological insulators with d-wave or $s_{\pm}$ -wave pairing induced by proximity effect proximity [21–23], and π-junction Rashba Layers with layer-dependent superconductor (SC) pairing [26]. From conventional topological point of view, a second order TSC or TSF has a d dimensional (dD) topologically trivial bulk. Its boundaries are stand-alone $d-1$ dimensional gapped SCs in essence. Therefore, the topologically protected Majorana states at corners or hinges naturally arise at the domain wall at the intersection of two adjacent edges or surfaces.

[4] Author to whom any correspondence should be addressed.

Rapid advances on synthetic gauge fields and magnetic fields in ultracold atoms provide an ideal platform for realizing novel quantum states of matter [27–34]. In a ultracold atom system, various degrees of freedom can be tuned, such as the tunneling strength between lattice sites on optical lattices, the Zeeman field, interaction strength, and etc. Ultracold atoms have been a powerful platform studying or simulating models originating from condensed matter systems for over one decade, where quantum degenerate neutral atom gases are used to simulate and explore physical regimes hard to be accessed by conventional solid-state systems. One remarkable advantage of this platform is free of disorders. In recent years remarkably experimental progress has been made including the realization of Hubbard model [35], BCS pairing [36] and various topological quantum matter [37], as well as transport measurements with cold atoms [38]. In particular, at this platform, $p_x + \mathrm{i}p_y$ SFs or non-Abelian s-wave SFs are proposed in spin–orbit coupled cold atoms [39], where Majorana zero modes localize at SF vortex cores or ends of the edge dislocations [40, 41]. Generally, by tuning the s -wave scattering length through Feshbach resonance technique, the s-wave attractive interaction between atoms can be fine tuned, so that s-wave Cooper pairing can be reached readily. However, in most of previous proposals [20–24, 26], the unconventional SC pairings (p-wave, d-wave, and $s_{\pm}$-wave, and etc.) are demanded for realizing the second order TSCs and TSFs. Naturally, an interesting question arises: can we reach an s-wave second order TSF and MCMs by making use of s-wave interaction?

Essentially, the emergence of MCMs originates from the Dirac-mass-sign changing at the corner in boundary theory for 2D TSCs. For example, in [21–23], the proximity-effect induced d -wave, and $s_{\pm}$-wave parings exhibit different features at distinct edges, and further give rise to MCMs. However, the conventional s-wave pairing is isotropic and then plays same role for all edges. It is necessary to introduce another parameter (the Zeeman field introduced below) to induce the changes for Dirac-mass sign at the intersection of adjacent edges.

The remaining of this paper is organized as follows. In section 2 we first introduce a quantum spin Hall insulator (QSHI) on a square lattice that may be realized in ultracold atoms. By tuning the s-wave interaction and the in-plane Zeeman field, the QSHI can be driven into a second order TSF. Numerical results confirm that MCMs exist in this topological phase. In section 3, by using the low energy edge theory, we unveil the emergence of MCMs. Finally, we conclude our discussions in section 4.

2. s-wave superfluid in correlated quantum spin Hall insulators

2.1. Quantum spin Hall insulators on a square lattice

We first consider a two-component Fermi gas loaded in a 2D optical lattice as sketched in figure 1. The single-particle Hamiltonian reads

$$\hat{H}_0 = \hat{H}_{\mathrm{NN}} + H_{\mathrm{NNN}} + H_{\mathrm{SZ}}, \tag{1}$$

which consists of the the nearest-neighbor (NN) hopping term $\hat{H}_{\mathrm{NN}}$, the next-nearest-neighbor (NNN) hopping term $\hat{H}_{\mathrm{NNN}}$, the staggered potential and the in-plane Zeeman term $\hat{H}_{\mathrm{SZ}}$:

$$\hat{H}_{\mathrm{NN}} = -\sum_{\vec{i}} \left(t_x a^{\dagger}_{\vec{i}} b_{\vec{i}\pm\vec{x}} - \mathrm{i}t_y a^{\dagger}_{\vec{i}} s_z b_{\vec{i}\pm\vec{y}} \right) + \mathrm{H.c.}, \tag{2}$$

$$\hat{H}_{\mathrm{NNN}} = -t' \sum_{\vec{i}} \left(a^{\dagger}_{\vec{i}} a_{\vec{i}+\vec{x}+\vec{y}} - a^{\dagger}_{\vec{i}} a_{\vec{i}+\vec{x}-\vec{y}} + b^{\dagger}_{\vec{i}} b_{\vec{i}+\vec{x}+\vec{y}} - b^{\dagger}_{\vec{i}} b_{\vec{i}+\vec{x}-\vec{y}} \right) + \mathrm{H.c.}, \tag{3}$$

$$\hat{H}_{\mathrm{SZ}} = m_0 \sum_{\vec{i}} \left(a^{\dagger}_{\vec{i}} a_{\vec{i}} - b^{\dagger}_{\vec{i}} b_{\vec{i}} \right) + h_x \sum_{\vec{i}} \left(a^{\dagger}_{\vec{i}} s_x a_{\vec{i}} + b^{\dagger}_{\vec{i}} s_x b_{\vec{i}} \right) - \mu \sum_{\vec{i}} \left(a^{\dagger}_{\vec{i}} a_{\vec{i}} + b^{\dagger}_{\vec{i}} b_{\vec{i}} \right), \tag{4}$$

where t_x and t_y are amplitudes for NN hopping terms along x and y, respectively. t' is the NNN hoping strength. The operator $a_{\vec{i}} = \left(a_{\vec{i},\uparrow}, a_{\vec{i},\downarrow} \right)$ ($b_{\vec{i}} = \left(b_{\vec{i},\uparrow}, b_{\vec{i},\downarrow} \right)$) annihilates a fermion with spin $\alpha = (\uparrow, \downarrow)$ at A (B)-sublattice site $\vec{i} = (i_x, i_y)$. m_0 is the staggered potential. μ is the chemical potential. $s_{x,y,z}$ are Pauli matrices acting on spin degrees of freedom. Hereafter, without loss of generality, the lattice spacing is set to be $|\vec{x}| = |\vec{y}| = 1$ throughout.

After Fourier transformation for the Hamiltonian, the equation (1) in momentum space is written as $\hat{H} = \sum_k C^{\dagger}_k H_0(k) C_k$, where the vector basis is $C^{\dagger}_k = \left(a^{\dagger}_{k,\uparrow}, b^{\dagger}_{k,\uparrow}, a^{\dagger}_{k,\downarrow}, b^{\dagger}_{k,\downarrow} \right)$, and the Hamiltonian matrix is

$$H_0(k) = \xi_k \sigma_z s_0 - 2t_x \cos k_x \sigma_x s_0 - 2t_y \cos k_y \sigma_y s_z - \mu \sigma_0 s_0 + h_x \sigma_0 s_x. \tag{5}$$

Here $\xi_k = -2t'[\cos(k_x + k_y) - \cos(k_x - k_y)] - m_0$. For simplicity, we choose $t_x = t_y = t$ and $\mu = 0$ in following discussions. h_x is a Zeeman field along the x direction. $\sigma_{x,y,z}$ are Pauli Matrices that act on sublattice degrees of freedom. σ_0 and s_0 are 2×2 unit matrices. The energy spectra for $H_0(k)$ is $e_k = \sqrt{(\gamma_k \pm h_x)^2 + (2t_y \cos k_y)^2}$ with $\gamma_k = \sqrt{\xi_k^2 + (2t_x \cos k_x)^2}$. At Dirac points $K = (\pi/2, \pi/2)$ and $K' = (\pi/2, -\pi/2)$, as illustrated in figure 1, the energy gap are $\min(|-4t' - m_0 + h_x|, |-4t' - m_0 - h_x|)$ and $\min(|4t' - m_0 + h_x|, |4t' - m_0 - h_x|)$, respectively.

In the absence of the Zeeman term ($h_x = 0$), $H_0(k)$ preserves time-reversal symmetry, i.e. $\mathcal{T} H_0(k) \mathcal{T}^{-1} = H_0(-k)$, where $\mathcal{T} = \mathrm{i}\sigma_0 s_y \mathcal{K}$. This system also has s_z conservation and we have spin $\uparrow$ and $\downarrow$ sectors, which also has symmetry $U(1) \times U(1)$, one $U(1)$ being the charge $U(1)$, and the other bing the $U(1)$ of s_z conservation. In fact, for the case with $|m_0| < 4|t'|$, the Hamiltonian H_0 are two quantum anomalous Hall insulators related to each other by the time-reversal operation. At this time, the system is characterized by nontrivial $\mathbb{Z}_2$ topological invariant 1. Each edge has a pair of

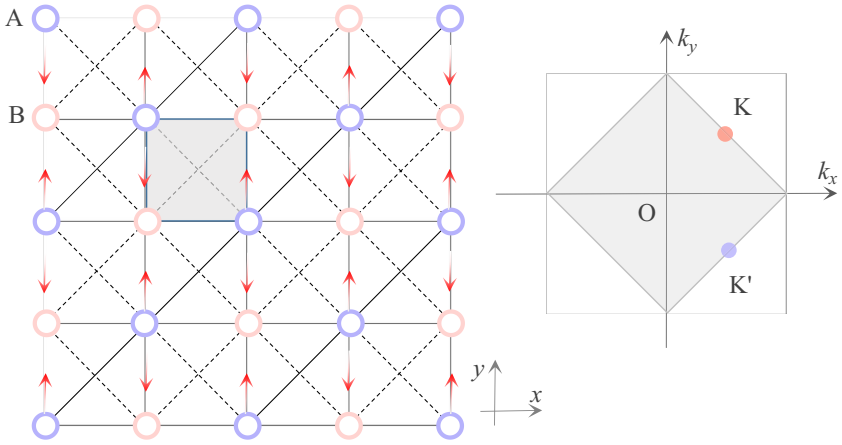

Figure 1. Left figure: The illustration of square optical lattices with laser induced gauge potentials. The particle with spin ↑ (↓) acquires 0 (0) phase when hopping along solid lines, acquires $\pi/2$ $(-\pi/2)$ phase when hopping along the red arrowed lines, and gets π (π) phase when hoping along dashed lines. Right figure: The illustration of reduced Brillouin zone indicated by the shaded region. $K = (\pi/2, \pi/2)$ and $K' = (\pi/2, -\pi/2)$ denote two inequivalent Dirac points.

counterpropagating gapless edge modes, which cross at $\mathcal{T}$-invariant point $k_x = \pm\pi/2$ or $k_y = \pm\pi/2$, as shown in figures 2(a) and (b). As long as $\mathcal{T}$ symmetry is preserved, each $\mathcal{T}$ invariant point must have two degenerate states according to Kramers theorem. There is no $\mathcal{T}$-invariant local perturbation that can couple the two branches of the single pair of edge states. Hence, to open a gap for a single pair of counterpropagating modes, the $\mathcal{T}$ symmetry for the system should be broken. We next consider a in-plane Zeeman field that breaks $\mathcal{T}$ symmetry. Due to $\{\sigma_y s_z, \sigma_0 s_x\} = 0$, the edge states along the y-direction are gapped, as confirmed in figure 2(d). However, because of $[\sigma_x s_0, \sigma_0 s_x] = 0$, gapless edge states still exist along the x-direction, as shown in figure 2(c). It indicates that the Zeeman field exhibits distinct features for edge states of the QSHI. Just because of this, in the following, we will see the Zeeman field plays a key role for implementing the second order TSFs.

2.2. SF phase transition for attractive Hubbard model

Consider the onsite interaction that can be tuned by Feshbach resonance technique, i.e.

$$\hat{H}_{\mathrm{U}} = -U \sum_i n_{i\uparrow} n_{i\downarrow}, \tag{6}$$

where $U > 0$ is the attractive interaction strength. As the interaction strength increases, the system enter a s-wave SF phase, where the s-wave pairing order parameter is $\Delta_{\mathrm{s}} = U \left\langle c^{\dagger}_{i\uparrow} c^{\dagger}_{i\downarrow} \right\rangle$. Then the total Hamiltonian now becomes $\hat{H} = \sum_{k>0} \Psi^{\dagger}_k H(k) \Psi_k + 2U\Delta^2_{\mathrm{s}}/N_{\mathrm{u}} - 2N_{\mathrm{u}}\mu$, where the basis $\Psi^{\dagger}_k = \left(C^{\dagger}_k, C_{-k}\right)$ and

$$\begin{aligned} H(k) = {} & \xi_k \sigma_z s_0 \tau_z - 2t_x \cos k_x \sigma_x s_0 \tau_z - 2t_y \cos k_y \sigma_y s_z \tau_0 \\ & + \Delta_{\mathrm{s}} \sigma_0 s_y \tau_y - \mu \sigma_0 s_0 \tau_z + h_x \sigma_0 s_x \tau_z. \end{aligned} \tag{7}$$

$\tau_{x,y,z}$ are Pauli matrices acting on the Nambu space. The energy spectra for $H(k)$ are given by $E_{k,\pm} = \sqrt{(\Gamma_k \pm h_x)^2 + (2t_x \cos k_y)^2}$ with $\Gamma_k = \sqrt{\Delta^2_{\mathrm{s}} + \xi^2_k + (2t_x \cos k_x)^2}$. The free energy per unit cell at temperature T is

$$F_u = -\frac{1}{N_{\mathrm{u}}} \sum_{k,v} \left(E_{k,v} - \frac{\Delta^2_{\mathrm{s}}}{U} + \mu + \frac{2}{\beta} \ln\left(1 + \mathrm{e}^{-\beta E_{k,v}}\right) \right) \tag{8}$$

with $\beta = 1/(k_{\mathrm{B}} T)$, where k_{B} is a Boltzmann constant, and N_{u} is the unit-cell number. For simplicity but without loss of generality, hereafter we consider the case with $\mu = 0$. By minimizing the free energy of the system, we obtain a self-consistent equation as

$$1 = \frac{U}{4N_{\mathrm{u}}} \sum_{\nu=\pm, k\in \mathrm{BZ}} \frac{1 + \nu/|\Gamma_k|}{E_{k,\nu}} \tanh\left(\beta E_{k,\nu}/2\right), \tag{9}$$

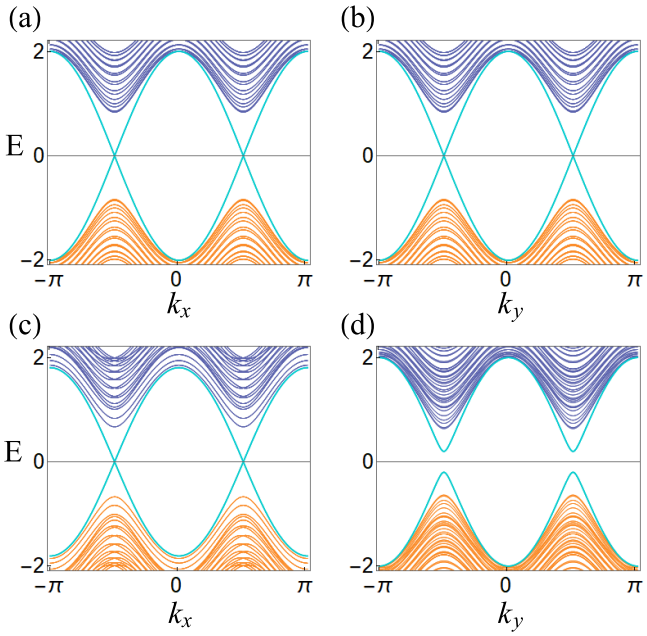

Figure 2. Energy level distributions on a stripe with open boundary condition along the y (x)-direction and periodic boundary condition along the x (y)-direction in (a)–(d). In (a) and (c), $h_x = .0$; (b) and (d) $h_x = .2$; parameters: $t = 1$, $t' = .2$, and $m_0 = \mu = .0$.

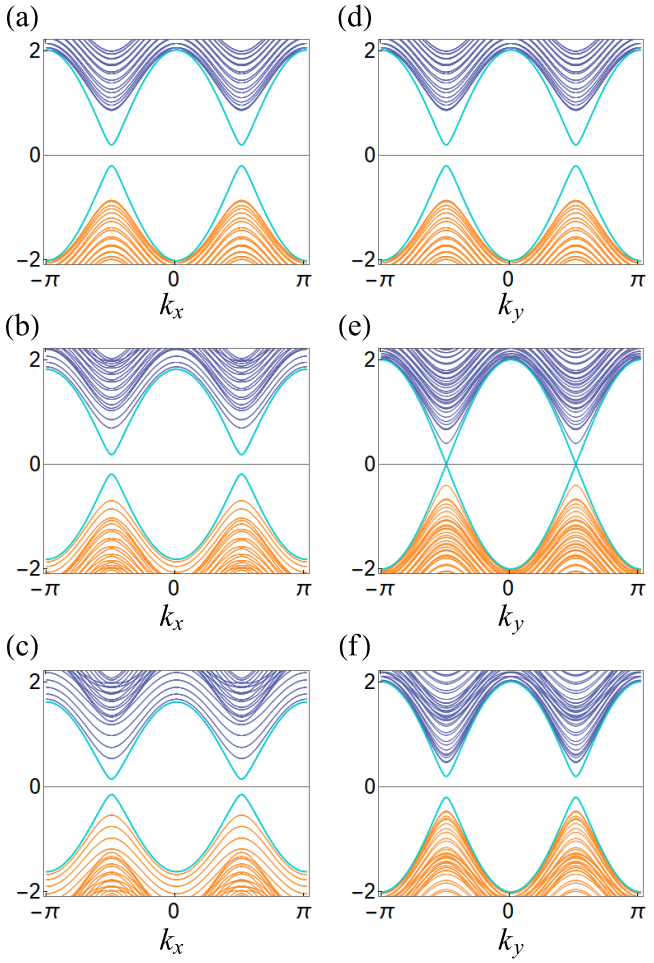

Figure 3. Energy level distributions on a stripe with open boundary condition along the y (x)-direction and periodic boundary condition along the x (y)-direction in (a)–(c) ((d)–(f)). (a) and (d) $h_x = .0$, $\Delta_s = .2$; (b) and (e) $h_x = .2$, $\Delta_s = .2$; (c) and (f) $h_x = .4$, $\Delta_s = .2$; Parameters: $t = 1$, $t' = .2$, and $m_0 = \mu = 0$.

where k runs over the Brillouin zone (BZ). By numerically solving the self-consistent equation (9), we find there exist three distinct phases: the insulator (I), metal (M), SF. In the following section, we will see SF consists of normal SF and second order topological SF phases.

2.3. Topological phase transitions and MCMs

First, consider the case with $h_x = 0$. As the onsite interaction increase, the system enters s-wave SF phase. The s-wave SF order gaps all helical edge modes of QSHI that propagate along the boundary, as shown in figures 3(a) and (d). Next, we turn on the in-plane Zeeman field. As the Zeeman field increases, as shown in figures 3(a)–(c), the energy gap along the x-direction remains; However, as shown in figures 3(d)–(f) the energy gap along the y-direction gradually decreases, closes at a critical value $h_{x,c} = \Delta_s$, and finally reopens. It indicates there is a topological transition (from trivial phase to topological phase) for edge states along the y-direction (This will be elucidated by using low-energy edge theory in the next section). With the consideration of this, we plot the global phase diagram in figure 4. There are two distinct SF

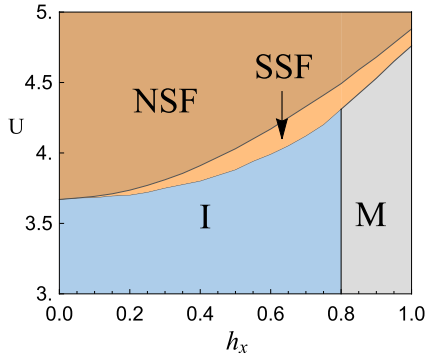

Figure 4. Global phase diagram: insulator (I), metal (M), normal superfluid (NSF), and second order topological SF (SSF) phases. Parameters $t = 1, t' = .2, m_0 = 0$ are used.

phase: Normal SFs (NSF) and second order SFs (SSF). This SSF here is an extrinsic one that can be characterized by a $\mathbb{Z}$ topological invariant from the topological transition for the edge states [42].

In fact, based on conventional topological classifications, the SSF is a bulk gapped trivial phase. So there are no gapless edge states propagating around the boundaries. However, Majorana corner states will emerge in this phase. We calculate the eigenenergy values for a square lattice with a size 60×60. The inset figure in figure 5(a) shows the symmetrical eigenenergies due to particle-hole symmetry. There are four zero energy modes in the gap. The probability density distributions of modes with zero energies, as illustrated in figure 5, show that each corner host one localized Majorana bound state known as MCM. Figure 5(b) shows the eigenenergies of a rectangle lattice with a size 60×40. Majorana corner states also remain.

We discuss the robustness of the Majorana corner modes. Firstly, the NN hopping amplitudes are slightly anisotropic, such as $t_x = 1$, $t_y = 1.2$, $t' = 0.2$. Figure 6(a) shows that the Majorana corner modes exist as long as in SSF phase, which indicates the MCMs are robust against the fluctuations of NN hopping. Second, the on-site potential is changed randomly according to $V_i = \zeta_i$, where ζ_i is a random variable distributed in a range $[-V_0/2, V_0/2]$, and $V_0 = 0.1$ describes the strength of a weak disorder. Figure 6(b) indicates the MCMs are also robust against weak disorders.

3. Low-energy edge theory in the continuum limit

To be explicit, we will unveil the emergence of MCMs from the SSF by using the low-energy edge theory in the continuum. With both SF pairing interaction and Zeeman field, the Hamiltonian $H_0(k)$ breaks time-reversal symmetry but respects particle-hole symmetry, $\mathcal{P}H_{\rm squ}(k)\mathcal{P}^{-1} = -H_{\rm squ}(-k)$ with $\mathcal{P} = \tau_x\mathcal{K}$. Without loss of generality, we supposed the pairing order parameter is a constant Δ_s for each lattice site. In the continuum limit, the low energy Hamiltonian up to the second order around Dirac point $K = (\pi/2, \pi/2)$ reads

$$H_{\rm squ}(k) = \left(\epsilon - 2t'k_x^2 - 2t'k_y^2\right)\sigma_z s_0 \tau_z + 2t_x k_x \sigma_x s_0 \tau_z + 2t_y k_y \sigma_y s_z \tau_0 + \Delta_s \sigma_0 s_y \tau_y + h_x \sigma_0 s_x \tau_z, \quad (10)$$

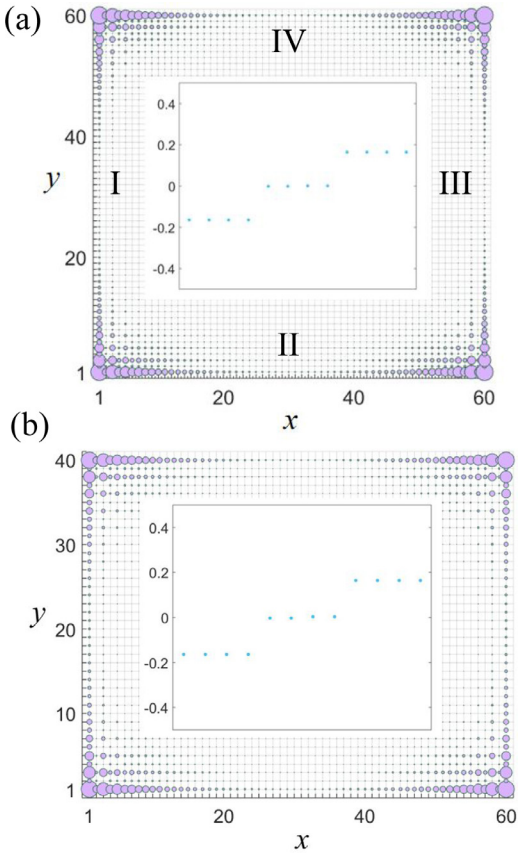

Figure 5. (a) Majorana modes at the corner of a square lattice with 60×60 sites. The radii of the purple spots are proportional to the square of the Majorana modes' wave function. The inset shows the eigenenergy values. (b) Majorana modes at the corner of a rectangle lattice with 60×40 sites. In (a) and (b), $t = 1, t' = .2$, $h_x = .4$, $\Delta_s = .2$, $m_0 = \mu = 0$ are used.

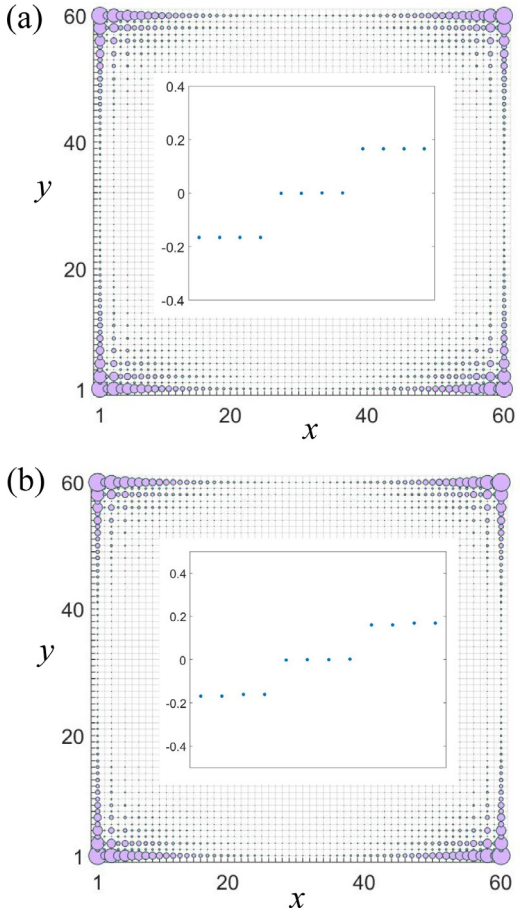

Figure 6. Majorana modes at the corner of a square lattice. The radii of the purple spots are proportional to the square of the Majorana modes' wave function. The inset shows the eigenenergy values. (a) $t_x = 1$, $t_y = 1.2$ and (b) $t_x = t_y = 1$. In both (a) and (b), parameters $t' = .2$, $h_x = .4$, $\Delta_s = .2$, $m_0 = \mu = 0$ are used.

where $\epsilon = 4t' - m_0 > 0$ is satisfied such that the insulator is in the Z_2 TI phase without the s-wave pairing and the Zeeman field. The four edges of a square lattice is labeled as I, II, III and IV as illustrated in figure 5(a). For the edge I, by replacing the momentum operator $k_x \to -\mathrm{i}\partial_x$, we decompose $H_{\rm squ}(k) = H_{\mathrm{I},M} + H_{\mathrm{I},P}$, where

$$\begin{aligned} H_{\mathrm{I},M}\left(-\mathrm{i}\partial_x, k_y\right) &= \left(\epsilon + 2t'\partial_x^2\right)\sigma_z s_0 \tau_z - 2it_x \partial_x \sigma_x s_0 \tau_z, \\ H_{\mathrm{I},P}\left(-\mathrm{i}\partial_x, k_y\right) &= -t' k_y^2 \sigma_z s_0 \tau_z + 2t_y k_y \sigma_y s_z \tau_0 \\ &\quad + \Delta_{\rm s} \sigma_0 s_y \tau_y + h_x \sigma_0 s_x \tau_z, \end{aligned} \tag{11}$$

of which $H_{\mathrm{I},M}$ is the main part, and $H_{\mathrm{I},P}$ is the the perturbation part when the pairing interaction is relatively small compared to the energy gap.

In the following, we first solve H_0, and then derive the the effective Hamiltonian for the edge I. For $H_{\mathrm{I},M}$, we have $\{H_{\mathrm{I},M}, \sigma_y s_z \tau_z\} = 0$, i.e. $H_{\mathrm{I},M}\sigma_y s_z \tau_z = -\sigma_y s_z \tau_z H_{\mathrm{I},M}$. We assume $H_{\mathrm{I},M}$ has zero energy solutions Ψ_a localized at the edge I. $\sigma_y s_z \tau_z \Psi_a$ are also the eigenstates for $H_{\mathrm{I},M}$. Hence, we choose eigenvectors ζ_β satisfying $\sigma_y s_z \tau_z\ \zeta_\beta = -\zeta_\beta$, where

$$\begin{aligned} \zeta_1 &= |\sigma_y = -1\rangle\,|s_z = +1\rangle\,|\tau_x = +1\rangle\,, \\ \zeta_2 &= |\sigma_y = +1\rangle\,|s_z = -1\rangle\,|\tau_x = +1\rangle\,, \\ \zeta_3 &= |\sigma_y = +1\rangle\,|s_z = +1\rangle\,|\tau_x = -1\rangle\,, \\ \zeta_4 &= |\sigma_y = -1\rangle\,|s_z = -1\rangle\,|\tau_x = -1\rangle\,. \end{aligned} \tag{12}$$

At this basis, there are four zero-energy bound states localized at the edge I: $\Psi_{i=1,2,3,4} = A\,(\sin\varsigma)\,\mathrm{e}^{-\frac{t_x}{2t'}x}\zeta_i$ with $\varsigma = \sqrt{-\left(\frac{t_x^2}{4t'^2} - \frac{\epsilon}{2t'}\right)}$ and A the normalization constant. For the perturbation term $H_{\mathrm{I},P}$, in the basis ζ_i, the low-energy effective edge Hamiltonian becomes

$$H_{\rm Edge,I} = it_y s_z \tau_0 \partial_y + \Delta_{\rm s} s_y \tau_y + h_x s_x \tau_z. \tag{13}$$

Following similar above procedure, we obtain low-energy edge Hamiltonian as

$$\begin{aligned} H_{\rm Edge,II} &= -\mathrm{i}t_x s_z \tau_0 \partial_x + \Delta_{\rm s} s_y \tau_y, \\ H_{\rm Edge,III} &= -\mathrm{i}t_y s_z \tau_0 \partial_y + \Delta_{\rm s} s_y \tau_y + h_x s_x \tau_z, \\ H_{\rm Edge,IV} &= it_x s_z \tau_0 \partial_x + \Delta_{\rm s} s_y \tau_y. \end{aligned}$$

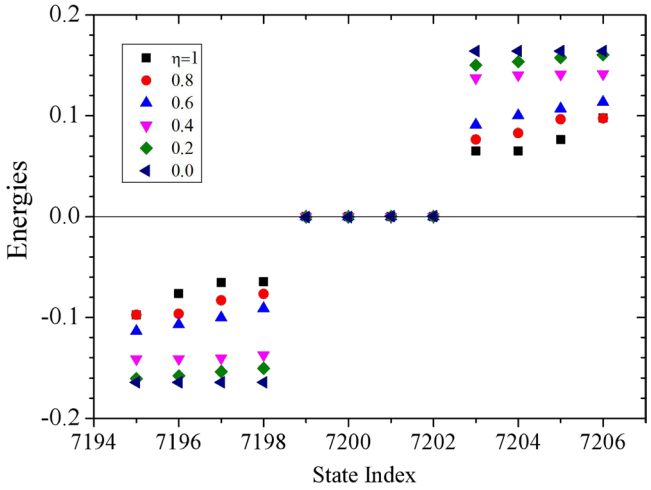

Figure 7. The eigenenergies of the second order topological superfluid with phase fluctuations on a square lattice with 60×60 sites. The inset denotes the strength parameters of phase fluctuations. Parameters $t = 1$, $t_0 = 0.2$, $h_x = 0.4, \Delta_0 = 0.2, m_0 = \mu = 0$ are used.

In the edge coordinate, the low-energy edge Hamiltonian is written as a concise form:

$$H_{\text{Edge}} = \mathrm{i}\lambda\left(l\right) s_z\tau_0\partial_l + \Delta_s s_y\tau_y + h\left(l\right) s_x\tau_z, \tag{14}$$

where $h\left(l\right) = h_x$,0 , h_x, 0 at boundaries I , II, III and IV, respectively. In the space

$$\begin{aligned}
\chi_1 &= \left|s_z = +1\right\rangle \left|\tau_x = +1\right\rangle, \\
\chi_2 &= \left|s_z = -1\right\rangle \left|\tau_x = -1\right\rangle, \\
\chi_3 &= \left|s_z = +1\right\rangle \left|\tau_x = -1\right\rangle, \\
\chi_4 &= \left|s_z = -1\right\rangle \left|\tau_x = +1\right\rangle,
\end{aligned} \tag{15}$$

the Hamiltonian H_{Edge} is rewritten as

$$H_{\text{Edge}} = -\mathrm{i}\lambda\left(l\right) s_z\tau_0\partial_x + \Delta_s s_x\tau_z + h\left(l\right) s_x\tau_0. \tag{16}$$

This Hamiltonian consists of two decoupled blocks. One block has Dirac mass $\Delta_s + h_x$, and the other has $\Delta_s - h_x$. If $\Delta_s.(\Delta_s - h_x) < 0$, then the Majorana corner mode naturally arises.

If a Zeeman field h_y along the y-direction is applied, the edge states for QSHI along the y-direction are also gapped due to $\left[\sigma_y s_z, \sigma_0 s_y\right]_+ = 0$. Taking similar steps, we can obtain an effective low-energy edge Hamiltonian as

$$H_{\text{Edge}} = -\mathrm{i}\lambda\left(l\right) s_z\tau_0\partial_x + \Delta_s s_y\tau_z + h\left(l\right) s_y\tau_0, \tag{17}$$

where $h\left(l\right) = 0$, h_y, 0, h_y at boundaries I, II, III and IV, respectively. It shows if $\Delta_s.(\Delta_s - h_y) < 0$, the Majorana corner mode also emerges. In general, for a in-plane Zeeman field $\vec{h} = (h_x, h_y, 0)$, the x-component and y-component Zeeman field both can gaps the gapless edge states for QSHI. Majorana corner states arise if $\left|\vec{h}\right| > \Delta_s$. For an out-of-plane Zeeman field h_z, it can not gap edge states for QSHIs due to $\left[\sigma_x s_0, \sigma_0 s_z\right] = 0$ and $\left[\sigma_y s_z, \sigma_0 s_z\right] = 0$. In this case, with s-wave SF order, the Dirac-mass sign does not change at the corner and no MCM emerges.

4. Discussion and conclusion

Previous studies showed zero-energy bound states localized around vortices in second order topological states [43], which originates from that the order parameter induces the sign change of Dirac mass term at the vortex. However, in our model the only superfluid order parameter could not change the sign of Dirac mass term. Explicitly, in the presence of superfluid vortex, the Dirac Mass term at the vortex core is h_x and far away form the core it becomes $h_x - \Delta_0$, where Δ_0 is the mean-field superfluid order-parameter profile of a vortex. In the second order topological superfluid phase, we have $h_x > \Delta_0$ (without loss of generality, we have assumed h_x, $\Delta_0 > 0$ here). So there is no sign change of Dirac mass term at the superfluid vortex. Therefore, the superfluid vortices in the second order topological superfluid do not host Majorana bound states.

To illustrate the robustness of Majorana corner modes to the phase fluctuations, we introduce the superfluid order parameters with phase fluctuations modeled as $\Delta_i = \Delta_0 \mathrm{e}^{\mathrm{i}\phi_i}$, where the random phase $\phi_i = 2\pi\eta\gamma_i$, η denotes the strength of phase fluctuations, and $\gamma_i \in [0, 1]$ is a random number. When $\eta = 0$, the superfluid order has a uniform phase with $\phi_i = 0$. When $\eta = 1$, the superfluid order suffers strongest phase fluctuations. We then numerically calculate eigenenergies of the second superfluid with random phases on a square lattice with 60×60 sites versus η. The numeric results have been shown in figure 7. It shows energies of bulk states may change as phase fluctuations become stronger, but Majorana corner modes are robust against phase fluctuations. In essence, the sign change of Dirac mass term at the corner leads to the emergence of Majorana corner mode. This relation also holds in the second order topological phase with phase fluctuations. So the Majorana corner modes are robust against phase fluctuations.

The high controllability of cold atoms provides a powerful platform to realize various novel quantum states of matter. The QSHI described by equation (1) may be realized via fermionic cold atoms (^{40}K) trapped in a spin-dependent optical lattice [35, 44]. By means of laser-induced gauge potentials, the phases of NN and NNN hopping can be reached [27, 45]. The on-site attractive interaction can be fine tuned through Feshbach resonance technique [46, 47]. The spatial-resolved radio-frequency spectroscopy that provides local information has been implemented in experiments for ultracold Fermi gases [48]. Using spatially resolved radio-frequency spectroscopy to measure the local density of states is a direct and convenient way to detect Majorana corner modes [49, 50], which is a cold-atom analog of scanning tunneling microscopy. In addition, the existence of the Majorana corner modes may be indirectly identified from the total density profile that can be measured via *in situ* or time-of-flight absorption imaging [35, 51].

In summary, we propose an s-wave SSF in a cold atom system. Three key ingredients consisting a QSHI, in-plane Zeeman field, and s-wave pairing are in this scheme.

The two dimensional QSHI hosts helical edge states protected by time-reversal symmetry. The in-plane Zeeman field gaps the helical edge sates along certain direction (y-direction in our scheme). Whereas the induced s-wave pairing by attractive interaction can open a gap for edge states along all boundaries. The combination of Zeeman field and SF order makes the Dirac mass signs for adjacent edges be opposite, and give rise to four MCMs on a square lattice. This work provides a new platform to reach Majorana zero modes and perform non-Abelian braidings.

Acknowledgments

This work is supported by NSFC under the Grant No. 11504285, and the Scientific Research Program Funded by Natural Science Basic Research Plan in Shaanxi Province of China (Program No. 2018JQ1058 and 2019JM-001), the Scientific Research Program Funded by Shaanxi Provincial Education Department under the Grant No. 19JK0391, and the scholarship from China Scholarship Council (CSC) (Program No. 201708615072).

ORCID iDs

Ya-Jie Wu https://orcid.org/0000-0003-2664-8094
Su-Peng Kou https://orcid.org/0000-0003-2225-3677

References

[1] Hasan M Z and Kane C L 2010 *Rev. Mod. Phys.* **82** 3045
[2] Qi X-L and Zhang S-C 2011 *Rev. Mod. Phys.* **83** 1057
[3] Zirnbauer M R 1996 *J. Math. Phys.* **37** 4986
[4] Altland A and Zirnbauer M R 1997 *Phys. Rev.* B **55** 1142
[5] Kitaev A Y 2009 *AIP Conf. Proc.* **22** 1134
[6] Fu L and Kane C L 2007 *Phys. Rev.* B **76** 045302
[7] Sato M 2009 *Phys. Rev.* B **79** 214526
[8] Hughes T L, Prodan E and Andrei Bernevig B 2011 *Phys. Rev.* B **83** 245132
[9] Shiozaki K and Sato M 2014 *Phys. Rev.* B **90** 165114
[10] Xu S-Y *et al* 2012 *Nat. Commun.* **3** 982
[11] Tanaka Y, Ren Z, Sato T, Nakayama K, Souma S, Takahashi T, Segawa K and Ando Y 2012 *Nat. Phys.* **8** 800
[12] Teo J C Y and Hughes T L 2013 *Phys. Rev. Lett.* **111** 047006
[13] Liu X-J, He J J and Law K T 2014 *Phys. Rev.* B **90** 235141
[14] Benalcazar W A, Teo J C Y and Hughes T L 2014 *Phys. Rev.* B **89** 224503
[15] Ueno Y, Yamakage A, Tanaka Y and Sato M 2013 *Phys. Rev. Lett.* **111** 087002
[16] Zhang F, Kane C L and Mele E J 2013 *Phys. Rev. Lett.* **111** 056403
[17] Langbehn J, Peng Y, Trifunovic L, von Oppen F and Brouwer P W 2017 *Phys. Rev. Lett.* **119** 246401
[18] Khalaf E 2018 *Phys. Rev.* B **97** 205136
[19] Wang Y, Lin M and Hughes T L 2018 *Phys. Rev.* B **98** 165144
[20] Zhu X 2018 *Phys. Rev.* B **97** 205134
[21] Yan Z, Song F and Wang Z 2018 *Phys. Rev. Lett.* **121** 096803
[22] Wang Q, Liu C-C, Lu Y-M and Zhang F 2018 *Phys. Rev. Lett.* **121** 186801
[23] Liu T, He J J and Nori F 2018 *Phys. Rev.* B **98** 245413
[24] Hsu C-H, Stano P, Klinovaja J and Loss D 2018 *Phys. Rev. Lett.* **121** 196801
[25] Wu Y-J, Hou J, Li Y-M, Luo X-W and Zhang C 2019 (arXiv:1905.08896)
[26] Volpez Y, Loss D and Klinovaja J 2019 *Phys. Rev. Lett.* **122** 126402
[27] Lin Y-J, Compton R L, Jiménez-García K, Porto J V and Spielman I B 2009 *Nature* **462** 628
[28] Lin Y-J, Jiménez-García K and Spielman I B 2011 *Nature* **471** 83
[29] Wang P *et al* 2012 *Phys. Rev. Lett.* **109** 095301
[30] Dalibard J, Gerbier F, Juzeliunas G and Ohberg P 2011 *Rev. Mod. Phys.* **83** 1523
[31] Carusotto I and Ciuti C 2013 *Rev. Mod. Phys.* **85** 299
[32] Goldman N, Juzeliunas G, Ohberg P and Spielman I B 2014 *Rep. Prog. Phys.* **77** 126401
[33] Wu Z *et al* 2016 *Science* **354** 83
[34] Song B *et al* 2018 *Sci. Adv.* **4** eaao4748
[35] Bloch I, Dalibard J and Zwerger W 2008 *Rev. Mod. Phys.* **80** 885
[36] Randeria M and Taylor E 2014 *Annu. Rev. Condens. Matter Phys.* **5** 209
[37] Goldman N, Budich J C and Zoller P 2016 *Nat. Phys.* **12** 639
[38] Krinner S, Esslinger T and Brantut J-P 2017 *J. Phys.: Condens. Matter* **29** 343003
[39] Sato M, Takahashi Y and Fujimoto S 2009 *Phys. Rev. Lett.* **103** 020401
[40] Bühler A, Lang N, Kraus C V, Möller G, Huber S D and Büchler H P 2014 *Nat. Commun.* **5** 4504
[41] Wu Y-J, Li N, Zhou J, Kou S-P and Yu J 2016 *J. Phys. B: At. Mol. Opt. Phys.* **49** 18530
[42] Geier M, Trifunovic L, Hoskam M and Brouwe P W 2018 *Phys. Rev.* B **97** 205135
[43] Rodriguez-Vega M, Kumar A and Seradjeh B 2019 *Phys. Rev.* B **100** 085138
[44] Hou J-M 2013 *Phys. Rev. Lett.* **111** 130403
[45] Aidelsburger M, Atala M, Nascimbène S, Trotzky S, Chen Y-A and Bloch I 2011 *Phys. Rev. Lett.* **107** 255301
[46] Khöler T, Góral K and Julienne P S 2006 *Rev. Mod. Phys.* **78** 1311
[47] Chin C, Grimm R, Julienne P and Tiesinga E 2010 *Rev. Mod. Phys.* **82** 1225
[48] Shin Y I, Schunck C H, Schirotzek A and Ketterle W 2007 *Phys. Rev. Lett.* **99** 090403
[49] Liu X-J 2015 *Phys. Rev.* A **91** 023610
[50] Liu X-J 2013 *Phys. Rev.* A **87** 013622
[51] Altman E, Demler E and Lukin M D 2004 *Phys. Rev.* A **70** 013603